Supplementary material for: Evaluation of PMIP2 and PMIP3 simulations of mid-Holocene climate in the Indo-Pacific, Australasian and Southern Ocean regions

Duncan Ackerley[1], Jessica Reeves[2], Cameron Barr[3,4], Helen Bostock[5], Kathryn Fitzsimmons[6], Michael-Shawn Fletcher[7], Chris Gouramanis[8], Helen McGregor[9], Scott Mooney[10], Steven J. Phipps[11], John Tibby[3,4], and Jonathan Tyler[3,4]

[1]ARC Centre of Excellence for Climate System Science, School of Earth, Atmosphere and Environment, Monash University, Victoria 3800, Australia
[2]Federation University, Faculty of Science and Technology, Mt Helen, Ballarat, Victoria 3353, Australia
[3]Department of Geography, Environment and Population. University of Adelaide, North Terrace, Adelaide, 5005.
[4]Sprigg Geobiology Centre. University of Adelaide, North Terrace, Adelaide, 5005.
[5]National Institute of Water and Atmospheric Research, 301 Evans Bay Parade, Greta Point, Wellington, New Zealand.
[6]Max Planck Research Group for Terrestrial Palaeoclimates, Climate Geochemistry, Max Planck Institute for Chemistry, Hahn-Meitner-Weg 1, 55128 Mainz, Germany
[7]School of Geography, University of Melbourne, Parkville, Victoria, Australia, 3010.
[8]Department of Geography, National University Of Singapore, 10 Kent Ridge Crescent, Singapore 119260
[9]School of Earth and Environmental Sciences, University of Wollongong, Northfields Ave, Wollongong NSW 2522 Australia
[10]School of Biological, Earth and Environmental Science, UNSW, Sydney 2052.
[11]Institute for Marine and Antarctic Studies, University of Tasmania, Hobart, Tasmania, Australia

Correspondence to: Duncan Ackerley (duncan.ackerley@monash.edu)

1 Introduction

This supplementary material document contains:

i A table of the models used in this study, their grid characteristics and relevant references (Table S1).

ii Regional differences in surface temperature, precipitation and 850 hPa flow over the same region as in Fig. 3 of the main text for the Southern Hemisphere "warm" and "cold" seasons (Figs. S1 and S2).

iii The difference in Pacific SST for both the 0 ka and 6 ka simulations relative to the 1979–2008 HadISST-derived mean (as referred to in Section 3.1.1 of the main text)—Fig. S3.

Should more seasonally-resolved proxies become available within each sub-domain of the southern Maritime Continent-Australasian-Southern Ocean region presented in this study (see Figs. 1 and 3 of the main text and, Figs. S1 and S2 below), then this supplement may help to judge whether the climate models agree or disagree with those proxy estimates.

2 Warm season characteristics

In this section, the months October to March (inclusive) are considered as the "warm" season (austral summer). This is when insolation in the SH peaks and is also the time of year when the Australian monsoon rainfall occurs (Sturman and Tapper, 2006). Conversely, this is also the season that the sub-tropical high-pressure belt is at its most southern extent and therefore the mid-latitudes are typically drier (Sturman and Tapper, 2006; Risbey et al., 2009). Therefore, in general, proxies that respond to moisture (such as fluvial and speleothem records) are expected to be more acutely tuned to the climatic state in the north of the Australasian region during the warm season. Furthermore, many of the biological proxies are representative of spring or summer conditions, the warm season reconstructions are better constrained (i.e. where the "sensor" is likely to be responding to climate signals) than during the autumn or winter.

2.1 Surface temperature

The differences between the 6 ka and 0ka ensemble-mean temperature is not significant and the model consensus is <60% in the TNW. Further south, in both the StA and TeE Australian zones there are lower ensemble mean surface temperatures (-0.18±0.12 K and -0.10±0.09 K, respectively) than in the tropics (Fig. S1(a)) at 6 ka. Furthermore, 78% of the models agree on reduced temperatures over StA; however, 65% agree in the TeE zone and the estimated temperature change is not statistically significant.

Surface temperatures are higher on average in the TeS zone (0.08±0.08 K); however, the change is not statistically significant and the model agreement is weak (56%). Conversely, the ensemble mean surface temperatures are higher in the 6 ka simulations for both the NSO (0.15±0.06 K) and SSO (0.26±0.08 K) zones (Fig. S1(a)). Moreover, model agreement (for higher 6 ka surface temperatures) is also high in both Southern Ocean zones (84% and 90%).

2.2 Precipitation

In the TNE zone there is lower precipitation at 6 ka (-3.39±1.85%, statistically significant) with 68% of the models agreeing (Fig. S1(b)). In TeE zone, 6 ka the ensemble mean precipitation amount is lower (-0.23±1.31%—non-significant) and model agreement on the changes is <60%. Conversely, there is evidence for higher precipitation at 6 ka in the TeS zone (2.14±1.39%—significant) with >70% model agreement. Finally, there are small differences in precipitation for 6 ka relative to 0 ka over both Southern Ocean zones (ensemble means of 0.58±0.52% and -0.11±0.42%, both non-significant) and model agreement is $\leq$56%.

2.3 Circulation

Ensemble mean easterly anomalies are present in the 6 ka simulations northward of the equator (Fig. S1(c)) and indicate a strengthening of the easterlies already present in the 0 ka simulations (blue colours). There are westerly anomalies between 0°S – 10°S, which are associated with stronger westerlies in the west of the domain and weakened easterlies in the east at 6 ka. The easterlies over Australia between 20°S – 30°S are stronger at 6 ka. There are also ensemble mean easterly anomalies

southward of 30°S; however, the anomalies are associated with a weakening of the westerly flow (indicated by the red colours Fig. S1(c)) at 6 ka.

3 Cold season characteristics

In this section, the months April to September (inclusive) are considered as the "cold" season (austral winter). This is when insolation in the SH is lowest during the year and also coincides with the dry season in northern Australia. Conversely, this is also the season that the mid-latitude westerly wind belt is at its most equatorward extent and therefore the mid-latitudes are typically wetter (Sturman and Tapper, 2006; Risbey et al., 2009). Therefore, precipitation-driven proxies are most strongly influenced by cool season anomalies in the higher latitudes. However, as several of the biological proxies are biased toward spring or summer conditions, the cool season reconstructions based on those archives may be poorly constrained.

3.1 Surface temperature

There is strong agreement (>80%) for lower surface temperatures in all tropical zones at 6 ka relative to 0 ka (Fig. S2(a)) and the magnitude of the temperature difference is larger in the northern zones (-0.31±0.05 K and -0.32±0.06 K) than the southern zones (-0.22±0.07 K and -0.23±0.05 K). Furthermore, greater than two-thirds of the models indicate lower temperatures at 6 ka in the TeE and TeS zones (-0.13±0.07 K and -0.19±0.06 K, both statistically significant), and the NSO (-0.07±0.05 K, not statistically significant). The only two regions with higher surface temperatures at 6 ka are the StA zone (0.03±0.08 K—non-significant) and the SSO (0.14±0.07 K—significant). The model agreement on increased temperatures is 84% for the SSO but is only 62% for StA.

3.2 Precipitation

Ensemble mean precipitation is not significantly different in all tropical regions except the TSW zone (Fig. S2(b)). In the TSW the ensemble mean change in precipitation is -2.69±1.37% (statistically significant with 81% of the models agreeing on the sign). Lower precipitation at 6 ka is also visible in all of the other regions southward of 20°S (Fig. S2(b)) but is only significant over the Southern Ocean. Precipitation is lower in the NSO and SSO zones by -3.17±0.97% and -2.57±0.45%, respectively (both statistically significant). Furthermore, ≥87% of the model simulations produce less precipitation at 6 ka relative to 0 ka in both Southern Ocean regions.

3.3 Circulation

Between 10°N – 15°S there is a strengthening of the easterlies at 6 ka relative to 0 ka (Fig. S2(c)). The only exception to the strengthened easterlies is in the north-east of the domain where the westerlies have weakened (north-westward of Borneo). There is little change to the 850 hPa circulation between 15°S – 35°S over the Australian continent. Finally, as with the previous time periods described above, there are weaker westerlies over the Southern Ocean at 6 ka relative to 0 ka (ensemble mean).

4 Cold tongue bias: PMIP models versus modern SST

The difference between the PMIP ensemble mean and HadISST (1979 – 2008) SSTs are plotted in Fig. S3(a) such that the HadISST averaging period corresponds with that of the circulation from ERA-Interim also plotted. The magnitude of the SST anomalies are larger ($\sim$-2.5 K) for the 0ka and 6 ka simulations relative to HadISST averaged over the modern era (Figs. S3(a) and (b), respectively); however, the errors are visible regardless of the averaging period and the interpretation above remains valid. The late 18^{th} Century (1870 – 1899) period is used for averaging instead of the modern period (1979 – 2008) in the main text (Fig. 4) as the impact of global warming from anthropogenic greenhouse gas emissions is reduced, which would otherwise make the simulated cold tongue bias appear artificially worse (greenhouse gas levels are set at pre-industrial in the PMIP simulations, see Table 1 in the main text). Fig. S3 is only included here for completeness.

References

Bao, Q., Lin, P., Zhou, T., Liu, Y., Yu, Y., Wu, G., He, B., He, J., Li, L., Li, J., Li, Y., Liu, H., Qiao, F., Song, Z., Wang, B., Wang, J., Wang, P., Wang, X., Wang, Z., Wu, B., Wu, T., Xu, Y., Yu, H., Zhao, W., Zheng, W., and Zhou, L.: The Flexible Global Ocean-Atmosphere-Land system model, Spectral Version 2: FGOALS-s2, Adv. Atmos. Sci., 30, 561–576, 2013.

Dufresne, J.-L., Foujols, M.-A., Denvil, S., Caubel, A., Marti, O., Aumont, O., Balkanski, Y., Bekki, S., Bellenger, H., Benshila, R., Bony, S., Bopp, L., Braconnot, P., Brockmann, P., Cadule, P., Cheruy, F., Codron, F., Cozic, A., Cugnet, D., Noblet, N., Duvel, J.-P., Ethé, C., Fairhead, L., Fichefet, T., Flavoni, S., Friedlingstein, P., Grandpeix, J.-Y., Guez, L., Guilyardi, E., Hauglustaine, D., Hourdin, F., Idelkadi, A., Ghattas, J., Joussaume, S., Kageyama, M., Krinner, G., Labetoulle, S., Lahellec, A., Lefebvre, M.-P., Lefevre, F., Levy, C., Li, Z., Lloyd, J., Lott, F., Madec, G., Mancip, M., Marchand, M., Masson, S., Meurdesoif, Y., Mignot, J., Musat, I., Parouty, S., Polcher, J., Rio, C., Schulz, M., Swingedouw, D., Szopa, S., Talandier, C., Terray, P., Viovy, N., and Vuichard, N.: Climate change projections using the IPSL-CM5 Earth System Model: from CMIP3 to CMIP5, Clim. Dynam., 40, 2123–2165, doi:10.1007/s00382-012-1636-1, http://dx.doi.org/10.1007/s00382-012-1636-1, 2013.

Gent, P. R., Danabasoglu, G., Donner, L. J., Holland, M. M., Hunke, E. C., Jayne, S. R., Lawrence, D. M., Neale, R. B., Rasch, P. J., Vertenstein, M., Worley, P. H., Yang, Z.-L., and Zhang, M.: The Community Climate System Model Version 4, J. Climate, 24, 4973–4991, 2011.

Giorgetta, M. A., Jungclaus, J., Reick, C. H., Legutke, S., Bader, J., Böttinger, M., Brovkin, V., Crueger, T., Esch, M., Fieg, K., Glushak, K., Gayler, V., Haak, H., Hollweg, H.-D., Ilyina, T., Kinne, S., Kornblueh, L., Matei, D., Mauritsen, T., Mikolajewicz, U., Mueller, W., Notz, D., Pithan, F., Raddatz, T., Rast, S., Redler, R., Roeckner, E., Schmidt, H., Schnur, R., Segschneider, J., Six, K. D., Stockhause, M., Timmreck, C., Wegner, J., Widmann, H., Wieners, K.-H., Claussen, M., Marotzke, J., and Stevens, B.: Climate and carbon cycle changes from 1850 to 2100 in MPI-ESM simulations for the Coupled Model Intercomparison Project phase 5, Journal of Advances in Modeling Earth Systems, 5, 572–597, 2013.

Gordon, C., Cooper, C., Senior, C. A., Banks, H., Gregory, J. M., Johns, T. C., Mitchell, J. F. B., and Wood, R. A.: The simulation of SST, sea ice extents and ocean heat transports in a version of the Hadley Centre coupled model without flux adjustments, Clim. Dynam., 16, 147–168, 2000.

Haak, H., Jungclaus, J., Mikolajewicz, U., and Latif, M.: Formation and propagation of great salinity anomalies, Geophys. Res. Lett., 30, 1473, 2003.

Hazeleger, W., Wang, X., Severijns, C., Ştefănescu, S., Bintanja, R., Sterl, A., Wyser, K., Semmler, T., Yang, S., van den Hurk, B., van Noije, T., van der Linden, E., and van der Wiel, K.: EC-Earth V2.2: description and validation of a new seamless earth system prediction model, Clim. Dynam., 39, 2611–2629, 2012.

Jacob, R., Schafer, C., Foster, I., Tobis, M., and Andersen, J.: Computational design and performance of the Fast Ocean Atmosphere Model: Version 1, in: The 2001 International Conference on Computational Science, pp. 175–184, 2001.

K-1-Model-Developers: K-1 Coupled GCM (MIROC description) I, Tech. rep., Center for Climate System Research (CCSR), University of Tokyo; National Institute for Environmental Studies (NIES); Frontier Research Center for Global Change (FRCGC), 2004.

Li, L., Lin, P., Yu, Y., Wang, B., Zhou, T., Liu, L., Liu, J., Bao, Q., Xu, S., Huang, W., Xia, K., Pu, Y., Dong, L., Shen, S., Liu, Y., Hu, N., Liu, M., Sun, W., Shi, X., Zheng, W., Wu, B., Song, M., Liu, H., Zhang, X., Wu, G., Xue, W., Huang, X., Yang, G., Song, Z., and Qiao, F.: The flexible global ocean-atmosphere-land system model, Grid-point Version 2: FGOALS-g2, Adv. Atmos. Sci., 30, 543–560, 2013.

Marsland, S. J., Haak, H., Jungclaus, J. H., Latif, M., and Roske, F.: The Max-Planck-Institute global ocean/sea ice model with orthogonal curvilinear coordinates, Ocean Model., 5, 91–127, 2003.

Marti, O., Braconnot, P., Bellier, J., Benshila, R., Bony, S., Brockmann, P., Cadule, P., Caubel, A., Denvil, S., Dufresne, J. L., Fairhead, L., Filiberti, M. A., Foujols, M.-A., Fichefet, T., Friedlingstein, P., Goosse, H., Grandpeix, J. Y., Hourdin, F., Krinner, G., Levy, C., Madec, G., Musat, I., deNoblet, N., Polcher, J., and Talandier, C.: The new IPSL climate system model: IPSL-CM4, Tech. Rep. 26, Note du Pole de Modelisation, iSSN 1288-1619, 2005.

Martin, G. M., Bellouin, N., Collins, W. J., Culverwell, I. D., Halloran, P. R., Hardiman, S. C., Hinton, T. J., Jones, C. D., McDonald, R. E., McLaren, A. J., O'Connor, F. M., Roberts, M. J., Rodriguez, J. M., Woodward, S., Best, M. J., Brooks, M. E., Brown, A. R., Butchart, N., Dearden, C., Derbyshire, S. H., Dharssi, I., Doutriaux-Boucher, M., Edwards, J. M., Falloon, P. D., Gedney, N., Gray, L. J., Hewitt, H. T., Hobson, M., Huddleston, M. R., Hughes, J., Ineson, S., Ingram, W. J., James, P. M., Johns, T. C., Johnson, C. E., Jones, A., Jones, C. P., Joshi, M. M., Keen, A. B., Liddicoat, S., Lock, A. P., Maidens, A. V., Manners, J. C., Milton, S. F., Rae, J. G. L., Ridley, J. K., Sellar, A., Senior, C. A., Totterdell, I. J., Verhoef, A., Vidale, P. L., and Wiltshire, A.: The HadGEM2 family of Met Office Unified Model climate configurations, Geosci. Model Dev., 4, 723–757, doi:10.5194/gmd-4-723-2011, http://www.geosci-model-dev.net/4/723/2011/, 2011.

Otto-Bliesner, B. L., Brady, E. C., Clauzet, G., Tomas, R., Levis, S., and a, Z. K.: Last Glacial Maximum and Holocene Climate in CCSM3, Journal of Climate, 19, 2526–2544, 2006.

Phipps, S. J., Rotstayn, L. D., Gordon, H. B., Roberts, J. L., Hirst, A. C., and Budd, W. F.: The CSIRO Mk3L climate system model version 1.0 – Part 1: Description and evaluation, Geosci. Model Dev., 4, 483–509, 2011.

Phipps, S. J., Rotstayn, L. D., Gordon, H. B., Roberts, J. L., Hirst, A. C., and Budd, W. F.: The CSIRO Mk3L climate system model version 1.0 – Part 2: Response to external forcings, Geosci. Model Dev., 5, 649–682, 2012.

Phipps, S. J., McGregor, H. V., Gergis, J., Gallant, A. J. E., Neukom, R., Stevenson, S., Ackerley, D., Brown, J. R., Fischer, M. J., and van Ommen, T. D.: Paleoclimate Data–Model Comparison and the Role of Climate Forcings over the Past 1500 Years, J. Climate, 26, 6915–6936, doi:10.1175/JCLI-D-12-00108.1, 2013.

Renssen, H., Goosse, H., Fichefet, T., Brovkin, V., Driesschaert, E., and Wolk, F.: Simulating the Holocene climate evolution at northern high latitudes using a coupled atmosphere-sea ice-ocean-vegetation model, Clim. Dynam., 24, 23–43, 2005.

Risbey, J. S., Pook, M. J., McIntosh, P. C., Wheeler, M. C., and Hendon, H. H.: On the Remote Drivers of Rainfall Variability in Australia, Mon. Wea. Rev., 137, 3233–3353, 2009.

Roeckner, E., Bauml, G., Bonaventura, L., Brokopf, R., Esch, M., Giorgetta, M., Hagemann, S., Kirchner, I., Kornblueh, L., Manzini, E., Rhodin, A., Schlese, U., Schulzweida, U., and Tompkins, A.: The atmospheric general circulation model ECHAM5, Part I: Model Description, Tech. Rep. 349, Max Planck Institute for Meteorology, Hamburg, 2003.

Rotstayn, L. D., Jeffrey, S. J., Collier, M. A., Dravitzki, S. M., Hirst, A. C., Syktus, J. I., and Wong, K. K.: Aerosol- and greenhouse gas-induced changes in summer rainfall and circulation in the Australasian Region: a study using single-forcing climate simulations, Atmos. Chem. Phys, 12, 6377–6404, 2012.

Schmidt, G. A., Ruedy, R., Hansen, J. E., Aleinov, I., Bell, N., Bauer, M., Bauer, S., Cairns, B., Canuto, V., Cheng, Y., Genio, A. D., Faluvegi, G., Friend, A. D., Hall, T. M., Hu, Y., Kelley, M., Kiang, N. Y., Koch, D., Lacis, A. A., Lerner, J., Lo, K. K., Miller, R. L., Nazarenko, L., Oinas, V., Perlwitz, J., Perlwitz, J., Rind, D., Romanou, A., Russell, G. L., Sato, M., Shindell, D. T., Stone, P. H., Sun, S., Tausnev, N., Thresher, D., and Yao, M.-S.: Present-Day Atmospheric Simulations Using GISS ModelE: Comparison to In Situ, Satellite, and Reanalysis Data, J. Climate, 19, 153–192, 2006.

Sturman, A. P. and Tapper, N. J.: The weather and climate of Australia and New Zealand, Oxford University Press, 2006.

Voldoire, A., Sanchez-Gomez, E., Salas y Mélia, D., Decharme, B., Cassou, C., Sénési, S., Valcke, S., Beau, I., Alias, A., Chevallier, M., Déqué, M., Deshayes, J., Douville, H., Fernandez, E., Madec, G., Maisonnave, E., Moine, M.-P., Planton, S., Saint-Martin, D., Szopa, S., Tyteca, S., Alkama, R., Belamari, S., Braun, A., Coquart, L., and Chauvin, F.: The CNRM-CM5.1 global climate model: description and basic evaluation, Clim. Dynam., 40, 2091–2121, 2013.

Watanabe, M., Suzuki, T., O'Ishi, R., Komuro, Y., Watanabe, S., Emori, S., Takemura, T., Chikira, M., Ogura, T., Sekiguchi, M., Takata, K., Yamazaki, S., Yokohata, T., Nozawa, T., Hasumi, H., Tatebe, H., and Kimoto, M.: Improved climate simulation by MIROC5: Mean states, variability and climate sensitivity, J. Climate, 23, 6312–6335, 2010.

Wu, T., Yu, R., Zhang, F., Wang, Z., Dong, M., Wang, L., Jin, X., Chen, D., and Li, L.: The Beijing Climate Center atmospheric general circulation model: description and its performance for the present-day climate, Clim. Dynam., pp. 123–147, 2010.

Yongqiang, Y., Rucong, Y., Xuehong, Z., and Hailong, L.: A flexible coupled ocean-atmosphere general circulation model, Adv. Atmos. Sci., 19, 169–190, 2002.

Yongqiang, Y., Xuehong, Z., and Yufu, G.: Global coupled ocean-atmosphere general circulation models in LASG/IAP, Adv. Atmos. Sci., 21, 444, 2004.

Yukimoto, S., Noda, A., Kitoh, A., Hosaka, M., Yoshimura, H., Uchiyama, T., Shibata, K., Arakawa, O., and Kusunoki, S.: Present-Day Climate and Climate Sensitivity in the Meteorological Research Institute Coupled GCM Version 2.3 (MRI-CGCM2.3), J. Meteor. Soc. Japan, 84, 333–363, 2006.

Yukimoto, S., Adachi, Y., Hosaka, M., Sakami, T., Yoshimura, H., Hirabara, M., Tanaka, T. Y., Shindo, E., Tsujino, H., Deushi, M., Mizuta, R., Yabu, S., Obata, A., Nakano, H., Koshiro, T., Ose, T., and Kitoh, A.: A new global climate model of the Meteorological Research Institute: MRI-CGCM3–Model description and basic performance, J. Meteor. Soc. Japan, 90A, 23–64, 2012.

Table S1. A list of the models used in this study, their original resolution / grid spacing and main references. The table is split into PMIP2 (1. – 18.) and PMIP3 (19. – 32.) models. For the PMIP2 models (1. – 18.), an asterisk (∗) denotes that the simulation is run with a dynamic vegetation scheme.

Model acronym	Atmosphere resolution Horiz. grid [levels]	Ocean resolution Horiz. grid [levels]	Main references
PMIP2			
1. CCSM3	T42 [26]	1° x 1° [40]	Otto-Bliesner et al. (2006)
2. CSIRO-Mk3L-1.0	R21 [18]	2.86125° x ∼1.59° [21]	Phipps et al. (2011, 2012)
3. CSIRO-Mk3L-1.1	R21 [18]	5.625° x ∼3.18° [21]	Phipps et al. (2011, 2012)
4. ECBILT-CLIO-VECODE	T21 [3]	3° x 3° [20]	Renssen et al. (2005)
5. ECBILT-CLIO-VECODE*	T21 [3]	3° x 3° [20]	Renssen et al. (2005)
6. ECHAM5-MPIOM1	T31 [19]	1.875° x 0.84° [40]	Roeckner et al. (2003); Marsland et al. (2003) Haak et al. (2003)
7. FGOALS-g1.0	2.8° x 2.8° [26]	1° x 1° [33]	Yongqiang et al. (2002, 2004)
8. FOAM	R15 [18]	2.8° x 1.4° [16]	Jacob et al. (2001)
9. FOAM*	R15 [18]	2.8° x 1.4° [16]	Jacob et al. (2001)
10. GISSmodelE	5° x 4° [12]	5° x 4° [18]	Schmidt et al. (2006)
11. UBRIS-HadCM3M2	3.75° x 2.5° [19]	1.25° x 1.25° [20]	Gordon et al. (2000)
12. UBRIS-HadCM3M2*	3.75° x 2.5° [19]	1.25° x 1.25° [20]	Gordon et al. (2000)
13. IPSL-CM4-V1-MR	3.75° x 2.5° [19]	2.0° x 0.5° [31]	Marti et al. (2005)
14. MIROC3.2	T42 [20]	1.4° x 0.5° [43]	K-1-Model-Developers (2004)
15. MRI-CGCM2.3fa	T42 [30]	2.5° x 0.5° [23]	Yukimoto et al. (2006)
16. MRI-CGCM2.3fa*	T42 [30]	2.5° x 0.5° [23]	Yukimoto et al. (2006)
17. MRI-CGCM2.3nfa	T42 [30]	2.5° x 0.5° [23]	Yukimoto et al. (2006)
18. MRI-CGCM2.3nfa*	T42 [30]	2.5° x 0.5° [23]	Yukimoto et al. (2006)
PMIP3			
19. BCC-CSM1-1	T42 [26]	1° x 1/3°–1° [40]	Wu et al. (2010)
20. CCSM4	1.25° x 0.9° [27]	1.125° x 0.27-0.64° [60]	Gent et al. (2011)
21. CNRM-CM5	1.875° x 1.875° [31]	0.7° x 0.7° [42]	Voldoire et al. (2013)
22. CSIRO-Mk3.6.0	T63 [18]	0.9° x 1.875° [31]	Rotstayn et al. (2012)
23. CSIRO-Mk3L-1.2	R21 [18]	2.86125° x ∼1.59° [21]	Phipps et al. (2013)
24. EC-EARTH2.2	T159 [62]	1° x 1° [31]	Hazeleger et al. (2012)
25. FGOALS-g2	2.8125° x 2.8125° [26]	1° x 0.5°–1° [30]	Li et al. (2013)
26. FGOASL-s2	R42 [26]	1° x 0.5°–1° [30]	Bao et al. (2013)
27. HadGEM2-CC	1.875° x 1.25° [60]	1.875° x 1.25° [40]	Martin et al. (2011)
28. HadGEM2-ES	1.875° x 1.25° [38]	1° x 1/3°–1° [30]	Martin et al. (2011)
29. IPSL-CM5A-LR	3.75° x 1.875° [39]	2° x 0.5°–2° [31]	Dufresne et al. (2013)
30. MIROC-ESM	T42 [80]	1.4° x 0.5°–1.4° [44]	Watanabe et al. (2010)
31. MPI-ESM-P	T63 [47]	1.5° x 1.5° [40]	Giorgetta et al. (2013)
32. MRI-CGCM3	T159 [48]	1° x 0.5° [50]	Yukimoto et al. (2012)

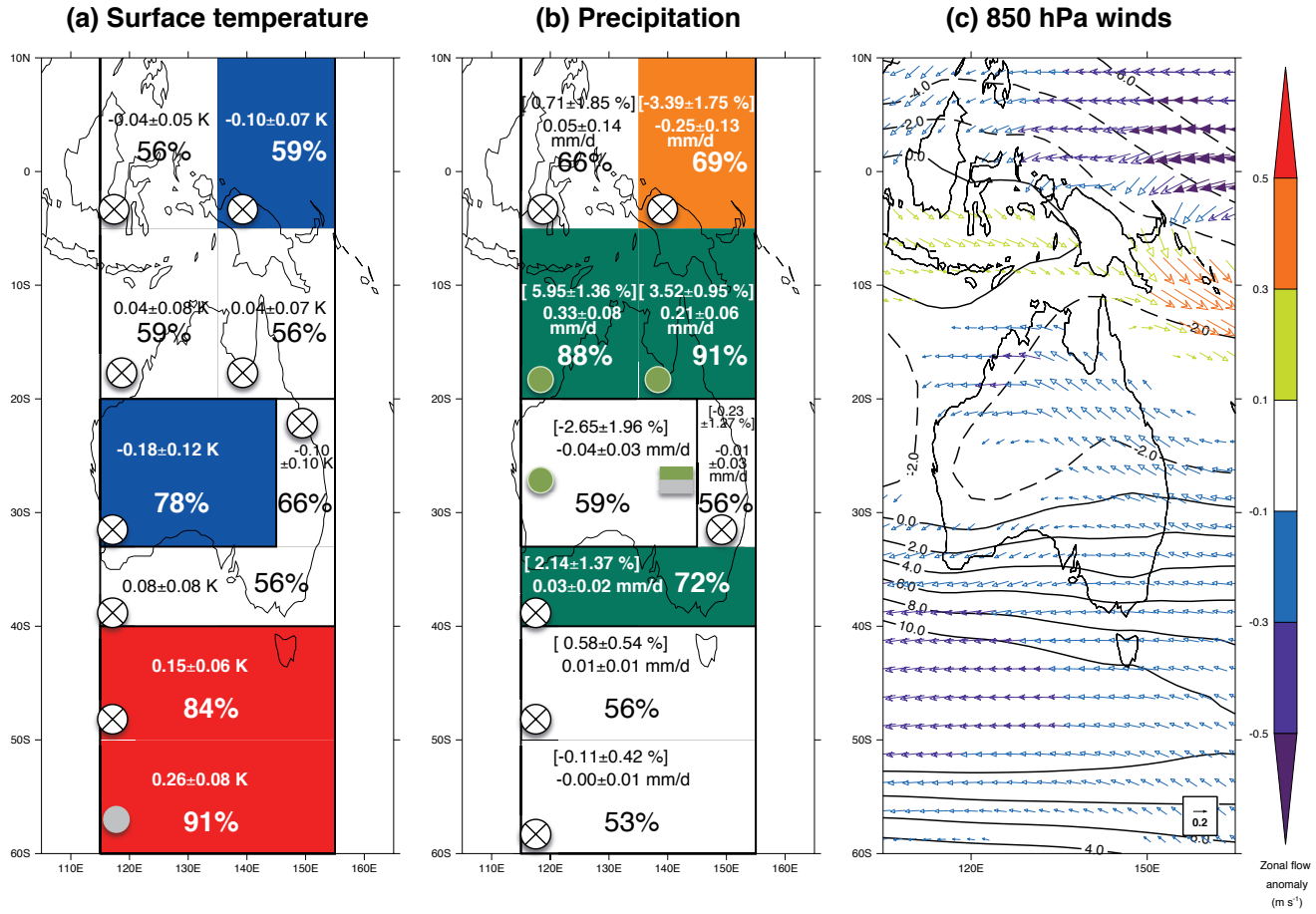

Figure S1. The ensemble and regional October to March mean differences in (a) surface temperature (K), (b) precipitation (mm day^{-1} and [%]) and (c) 850 hPa circulation (m s^{-1}) for the 6 ka simulations relative to the 0 ka simulations. In (a) blue shading (circles) represents lower area-averaged surface temperature and red shading (circles) indicates higher at 6 ka from PMIP (proxy) estimates. In (b), orange shading (circles) indicates lower area averaged precipitation and green shading (circles) indicates higher at 6 ka from PMIP (proxy) estimates. Grey circles indicate that proxy-derived temperature and/or precipitation at 6 ka was equivalent to 0 ka and unshaded boxes indicate changes in temperature and/or precipitation that are not statistically significant ($p>0.05$) in the models. *N.B. In (b) the green/grey rectangles denote the proxy-derived precipitation change in the northern and southern halves of the StA zone, respectively*. In both (a) and (b) the values of the ensemble mean changes and the percentages of models that agree on the sign (positive or negative) of the ensemble mean temperature or precipitation differences are given. Furthermore, circles with an "X" through the middle indicate no proxy data available (both temperature and precipitation). In (c) solid and dashed contour lines indicate mean westerly and easterly flow (respectively) in the 0 ka simulations and the overlaid arrows show vector wind anomalies for 6 ka relative to 0 ka (arrow length and colour is proportional to wind anomaly strength—0.2 m s^{-1} is the plotted reference value for the vector length).

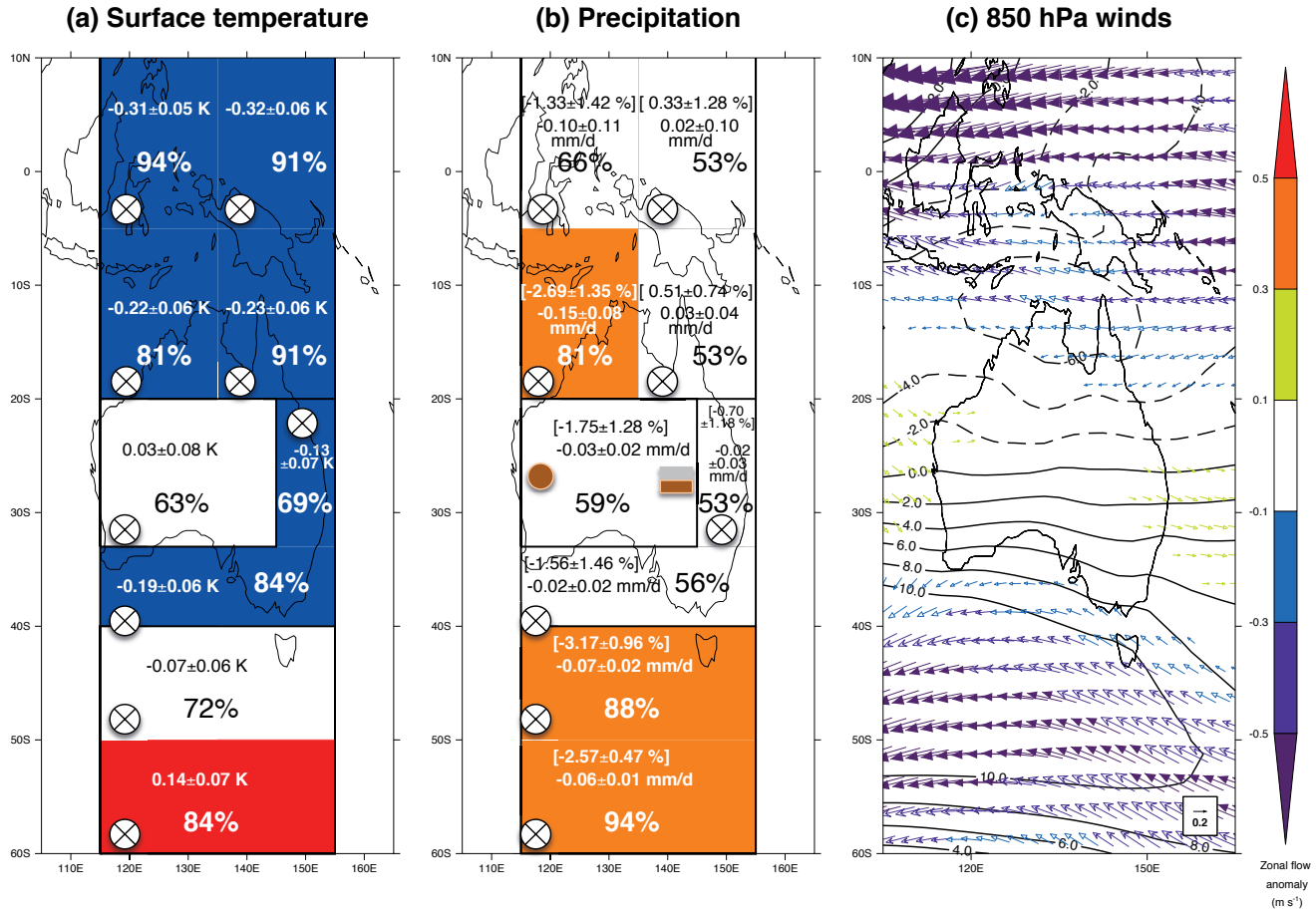

Figure S2. The ensemble and regional April to September mean differences in (a) surface temperature (K), (b) precipitation (mm day^{-1} and [%]) and (c) 850 hPa circulation (m s^{-1}) for the 6 ka simulations relative to the 0 ka simulations. In (a) blue shading (circles) represents lower area-averaged surface temperature and red shading (circles) indicates higher at 6 ka from PMIP (proxy) estimates. In (b), orange shading (circles) indicates lower area averaged precipitation and green shading (circles) indicates higher at 6 ka from PMIP (proxy) estimates. Grey circles indicate that proxy-derived temperature and/or precipitation at 6 ka was equivalent to 0 ka and unshaded boxes indicate changes in temperature and/or precipitation that are not statistically significant (p>0.05) in the models. *N.B. In (b) the grey/orange rectangles denote the proxy-derived precipitation change in the northern and southern halves of the StA zone, respectively*. In both (a) and (b) the values of the ensemble mean changes and the percentages of models that agree on the sign (positive or negative) of the ensemble mean temperature or precipitation differences are given. Furthermore, circles with an "X" through the middle indicate no proxy data available (both temperature and precipitation). In (c) solid and dashed contour lines indicate mean westerly and easterly flow (respectively) in the 0 ka simulations and the overlaid arrows show vector wind anomalies for 6 ka relative to 0 ka (arrow length and colour is proportional to wind anomaly strength—0.2 m s^{-1} is the plotted reference value for the vector length).

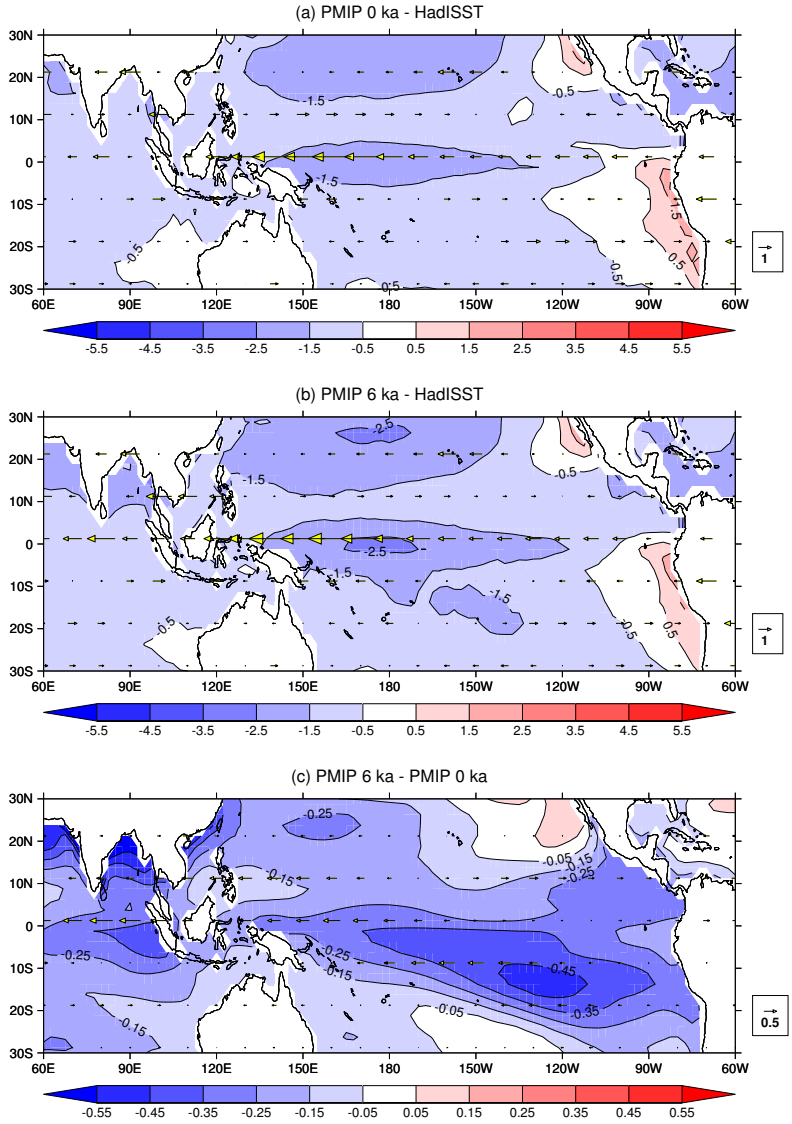

Figure S3. The multi-model mean difference in SST (shading, K) and 850 hPa flow (arrows, m s^{-1}) for the 0 ka simulations relative to HadISST (1979 – 2008 average) and ERA-Interim (1979 – 2008 average), respectively. (b) the same as (a) except for the 6 ka simulations. (c) The multi-model mean difference in SST and 850 hPa flow for the 6 ka simulations relative to the 0 ka simulations.